*Supplementary Information*

# Influence of Structure-Activity Relationships on Through-Space Intervalence Charge Transfer in Metal-Organic Frameworks with Cofacial Redox Active Units

Bowen Ding, Carol Hua, Cameron J. Kepert* and Deanna M. D'Alessandro*

School of Chemistry, University of Sydney, NSW 2006, Australia

*Corresponding author email: cameron.kepert@sydney.edu.au; deanna.dalessandro@sydney.edu.au

## SYNTHESIS

**4-(4-Pyridinyl)-benzaldehyde** was prepared following a modified literature procedure.[1] To degassed 1,4-dioxane (90 mL) and $H_2O$ (10 mL), anhydrous $K_2CO_3$ (6.0 g, 43 mmol), 4-bromobenzaldehyde (1.0 g, 5.4 mmol), pyridine-4-boronic acid (0.80 g, 6.5 mmol) and tetrakistriphenylphosphinepalladium(0) (0.33 g, 0.29 mmol) were added. This was heated to reflux under $N_2$ with stirring for 24 h, after which the reaction mixture was cooled to RT, and the solvent removed by rotary evaporation. The residue was then partitioned between DCM (150 mL) and $H_2O$ (150 mL), and the organic phase collected. The aqueous phase was extracted with DCM (2 × 50 mL), and the combined organic phases dried with $MgSO_4$, after which the solvent was removed by rotary evaporation. The resulting off white residue was purified by silica gel column chromatography, eluting with 19:1 DCM/MeOH followed by 19:1:2 DCM/MeOH/$Et_3N$, to yield 4-(4-pyridinyl)-benzaldehyde as an off white solid (0.97 g, 98%, m.p. 75-77 °C). $^1$H NMR ($CDCl_3$, 300 MHz): δ 10.01 (*s*, 1H), 8,73 (*s*, 2H), 8.01 (*d*, $^3J_{\text{H-H}}$ = 8.1 Hz, 2H), 7.80 (*d*, $^3J_{\text{H-H}}$ = 8.1 Hz, 2H), 7.55 (*d*, $^3J_{\text{H-H}}$ = 4.8 Hz, 2H) ppm. $^{13}$C{$^1$H} NMR ($CDCl_3$, 75 MHz): δ 191.8, 150.7, 147.1, 144.2, 136.7, 130.6, 127.9, 121.9 ppm. ESI-MS (ESI$^+$, MeOH): 184 (Calculated $[M+H]^+$ = 184.2, 100%) amu.

**2,5-*Bis*(4-(4-pyridyl)phenyl)thiazolo[5,4-*d*]thiazole (DPPTzTz)** Dithiooxamide (0.29 g, 2.4 mmol) and 4-(4-pyridinyl)-benzaldehyde (0.93 g, 5.1 mmol) were suspended in DMF (25 mL) and heated to reflux with stirring for 3 h under $N_2$. The reaction mixture was cooled to RT, chilled in an ice bath, and the resulting yellow solid isolated by suction filtration. The yellow solid was washed with cold DMF followed by $H_2O$. This was dried *in vacuo* to obtain DPPTzTz as a dull yellow solid (0.46 g, 42%, m.p. ≥ 300 °C). $^1$H NMR (*d*-TFA, 400 MHz): δ 8.84 (*d*, $^3J_{\text{H-H}}$ = 5.6 Hz, 4H), 8.35 (*d*, $^3J_{\text{H-H}}$ = 5.2 Hz, 4H), 8.26 (*d*, $^3J_{\text{H-H}}$ = 8.0 Hz, 4H), 8.06 (*d*, $^3J_{\text{H-H}}$ = 8.0 Hz, 4H) ppm. $^{13}$C{$^1$H} NMR (*d*-TFA, 100 MHz): δ 175.0, 160.8, 150.4, 143.7, 140.3, 136.1, 131.4, 130.8, 127.3 ppm. ESI-MS (ESI$^+$, $CH_3CN$): 449 (Calculated $[M+H]^+$ = 449.6, 100%) amu. Elemental analysis: Found, %: C 69.56, H 3.53, N 12.40. Calculated for $C_{26}H_{16}N_4S_2$, %: C 69.62, H 3.60, N 12.49.

**2,5-Dibromoselenophene** was synthesised according to literature procedure[2] and obtained as a yellow oil (9.3 g, 85%) $^1$H NMR ($CDCl_3$, 300 MHz): δ 7.00 (s, 1H) ppm. $^{13}$C{$^1$H} NMR ($CDCl_3$, 75 MHz): δ 133.1, 115.8 ppm.

**Selenophene-2,5-dicarboxylic acid (SDC)** 2,5-Dibromoselenophene (2.0 g, 6.9 mmol) was dissolved in dry THF (70 mL) and the resulting solution cooled to -78 °C, after which *n*-BuLi (2.5 M in hexanes, 5.8 mL, 14.5 mmol) was added dropwise with stirring yielding a colour change from yellow to light orange to light brown to green. This was left to stir at -78 °C for 10 mins, after which $CO_2$ was bubbled through the solution for 1 h, resulting in the formation of a cream solid. The reaction mixture was then warmed to RT, after which HCl (1 M, 100 mL) was added carefully resulting in slight effervescence. The yellow-orange organic phase was isolated, and the aqueous phase extracted further with $Et_2O$ (3 × 50 mL). The organic fractions were then combined and dried with $MgSO_4$, after which the solvent was removed by rotary evaporation to yield a yellow-orange solid. The crude product was washed with $CHCl_3$ (50 mL) to yield selenophene-2.5-dicarboxylic acid as a cream solid (1.1 g, 74%) $^1$H NMR (DMSO-$d_6$, 400 MHz): δ 13.49 (*br s*, 2H), 7.94 (*s*, 2H) ppm. $^{13}$C{$^1$H} NMR (DMSO-$d_6$, 100 MHz): δ 163.7, 146.2, 135.6 ppm. ESI-MS (ESI$^-$, MeOH): 218 (Calculated $[M-H]^-$ = 218.1, 100%) amu. Elemental analysis: Found, %: C 33.03, H 1.55, N <0.05. Calculated for $C_6H_4O_4Se$, %: C 32.89, H 1.83, N 0.00.

## CRYSTALLOGRAPHY TABLES

**Table S1**. Crystal data for **1-Zn**.

| Parameter | |
|---|---|
| Formula | $C_{64}H_{36}N_8O_8S_4Se_2Zn_2$ |
| M/g mol$^{-1}$ | 1461.91 |
| Temperature (K) | 100(2) |
| Crystal system | monoclinic |
| Space group | $P2_1/c$ (#14) |
| Crystal size (mm$^3$) | 0.080 × 0.04 × 0.030 |
| Crystal colour | Yellow |
| Crystal Habit | Block |
| a (Å) | 25.811(5) |
| b (Å) | 18.453(4) |
| c (Å) | 15.943(3) |
| $\beta$ (°) | 90.91(3) |
| V (Å$^3$) | 7593(3) |
| Z | 4 |
| $\rho_{calc}$ (mg mm$^{-3}$) | 1.279 |
| λ(Synchrotron) | 0.71073 Å |
| μ(Synchrotron) | 1.751 mm$^{-1}$ |
| $2\theta_{max}$ (°) | 63.70 |
| hkl range | -35 35, -23 23, -20 20 |
| Reflections collected | 142509/21132 [R(int) = 0.0995] |
| Data/Parameters | 13593/862 |
| Final R indexes [all data] | $R_1$ = 0.0580, $wR_2$ = 0.1551 |
| Goodness-of-fit on $F^2$ | 0.955 |
| Residual Extrema | -1.787, 0.891 e$^-$Å$^{-3}$ |

$R1 = \Sigma(|F_o| - |F_c|)/\Sigma(|F_o|)$; $wR_2 = [\Sigma\{w(F_o^2 - F_c^2)^2\}/\Sigma\{w(F_o^2)^2\}]^{1/2}$, $wR2 = (\Sigma w(F_o^2 - F_c^2)^2/\Sigma(wF_c^2)^2)^{1/2}$ all reflections $w=1/[\sigma^2(F_o^2)+(0.0922P)^2]$ where $P=(F_o^2+2F_c^2)/3$

**Table S2**. Crystal data for **2-Cd**.

| Parameter | |
|---|---|
| Formula | $C_{128}H_{72}Cd_4N_{16}O_{16}S_8Se_4$ |
| M/g mol$^{-1}$ | 3111.93 |
| Temperature (K) | 100(2) |
| Crystal system | triclinic |
| Space group | *P*-1 (#2) |
| Crystal size (mm$^3$) | 0.080 × 0.06 × 0.040 |
| Crystal colour | Yellow |
| Crystal Habit | Block |
| a (Å) | 15.868(3) |
| b (Å) | 19.123(4) |
| c (Å) | 26.124(5) |
| α (°) | 82.02(3) |
| β (°) | 87.25(3) |
| γ (°) | 89.73(3) |
| V (Å$^3$) | 7841(3) |
| Z | 2 |
| $\rho_{calc}$ (mg mm$^{-3}$) | 1.318 |
| λ(Synchrotron) | 0.71073 Å |
| μ(Synchrotron) | 1.626 mm$^{-1}$ |
| $2\theta_{max}$ (°) | 58.43 |
| $T(XDS)_{min, max}$ | 0.3564, 0.4318 |
| hkl range | -21 21, -25 25, -32 32 |
| Reflections collected | 109850/28473 [R(int) = 0.0907] |
| Data/Parameters | 18399/1575 |
| Final R indexes [all data] | $R_1 = 0.1193$, $wR_2 = 0.3490$ |
| Goodness-of-fit on F$^2$ | 1.286 |
| Residual Extrema | -2.335, 4.312 e$^-$Å$^{-3}$ |

$R1 = \Sigma(|F_o| - |F_c|)/\Sigma(|F_o|)$; $wR_2 = [\Sigma\{w(F_o^2 - F_c^2)^2\}/\Sigma\{w(F_o^2)^2\}]^{1/2}$, $wR2 = (\Sigma w(F_o^2 - F_c^2)^2/\Sigma(wF_c^2)^2)^{1/2}$ all reflections $w=1/[\sigma^2(F_o^2)+(0.2000P)^2]$ where $P=(F_o^2+2F_c^2)/3$

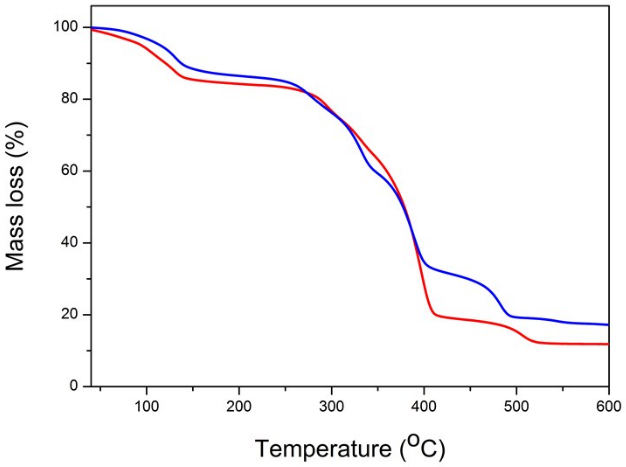

**Figure S1**. Thermogravimetric analysis of **1-Zn** (red) and **2-Cd** (blue) showing loss of solvent at 100 °C and framework degradation at 300 – 400 °C.

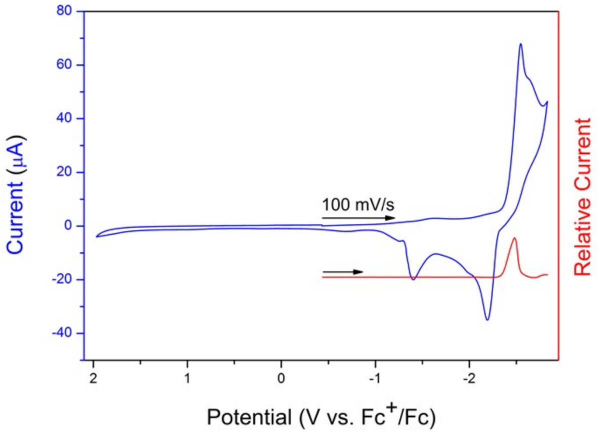

**Figure S2**. Solid state CV (blue) and SQW (red) electrochemistry in 0.1 M [$n$-$Bu_4N$]$PF_6$ / MeCN for DPPTzTz.

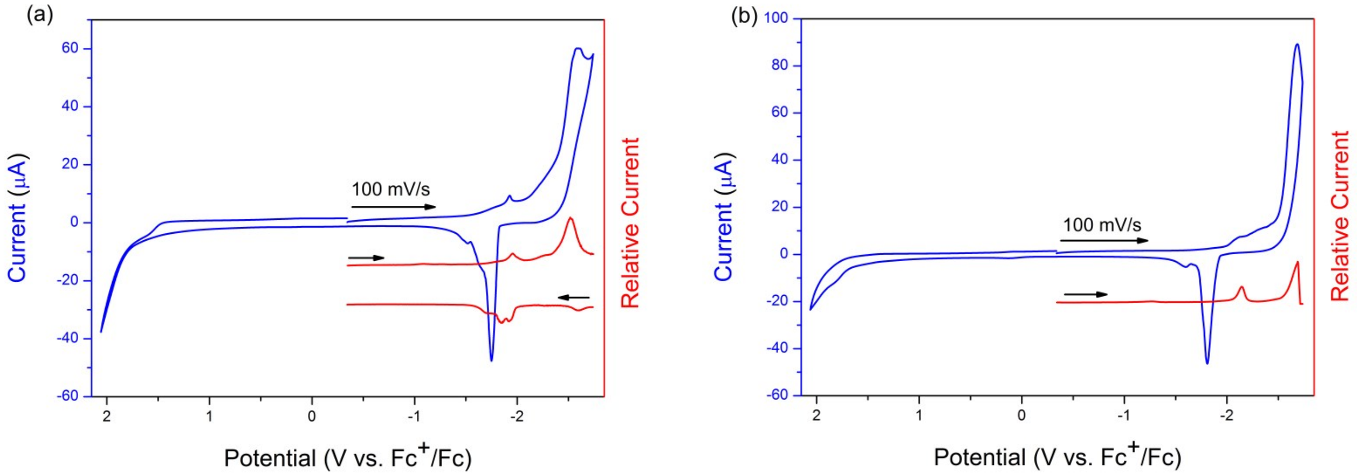

**Figure S3**. Solid state CV (blue) and SQW (red) electrochemistry in 0.1 M [$n$-$Bu_4N$]$PF_6$ / MeCN for (a) **1-Zn** and (b) **2-Cd**.

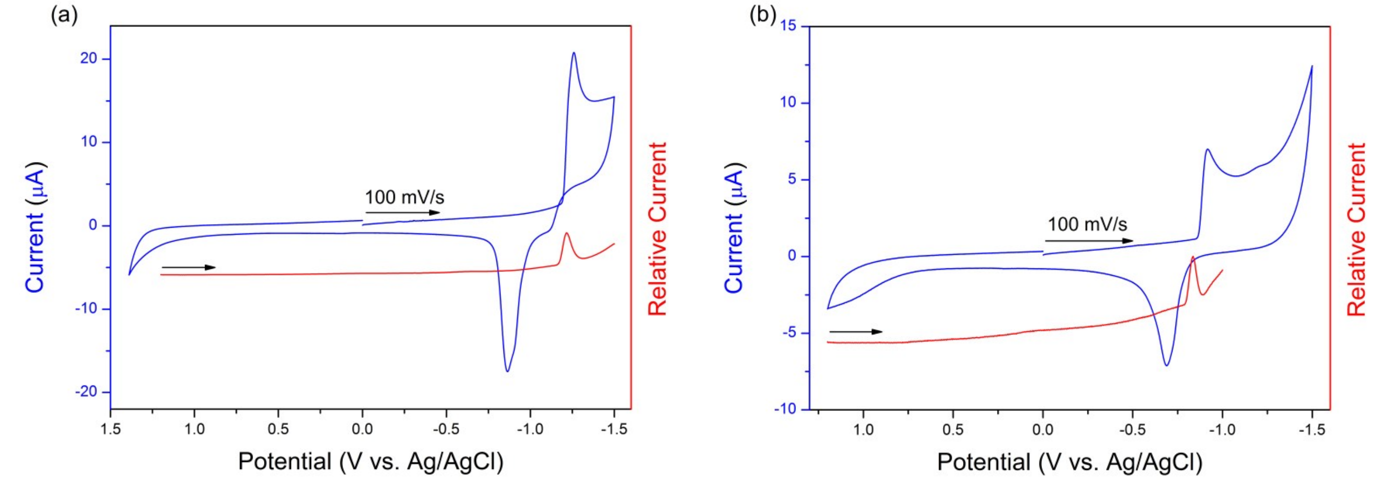

**Figure S4**. Solid state CV (blue) and SQW (red) electrochemistry in 0.1 M KCl / $H_2O$ for (a) **1-Zn** and (b) **2-Cd**.

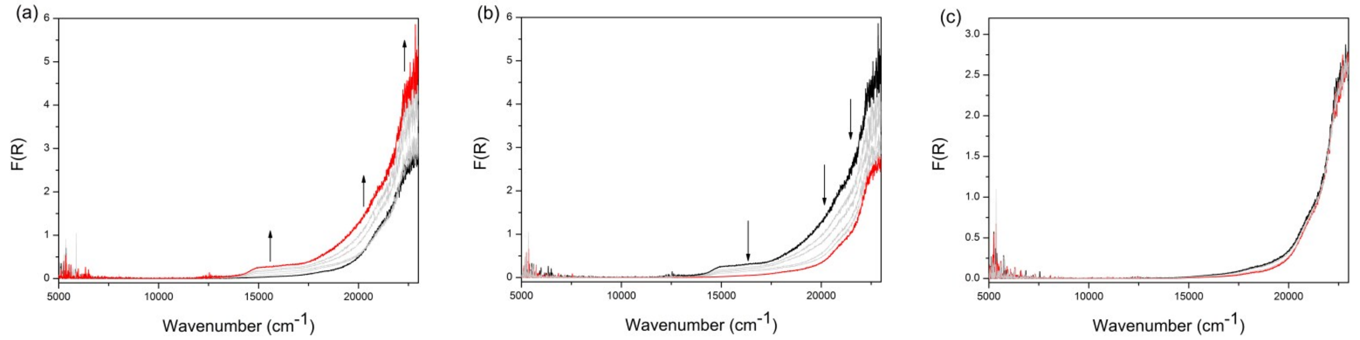

**Figure S5**. Solid state UV-Vis-NIR SEC of DPPTzTz in 0.1 M [*n*-$Bu_4N$]$PF_6$ / MeCN with arrows indicating spectral progression of bands at an applied potential of (a) -2.2 V whereupon the monoanion radical state is being accessed; (b) -2.4 V whereupon the dianion state is being accessed; and (c) upon returning to 0 V, against Ag/Ag$^+$.

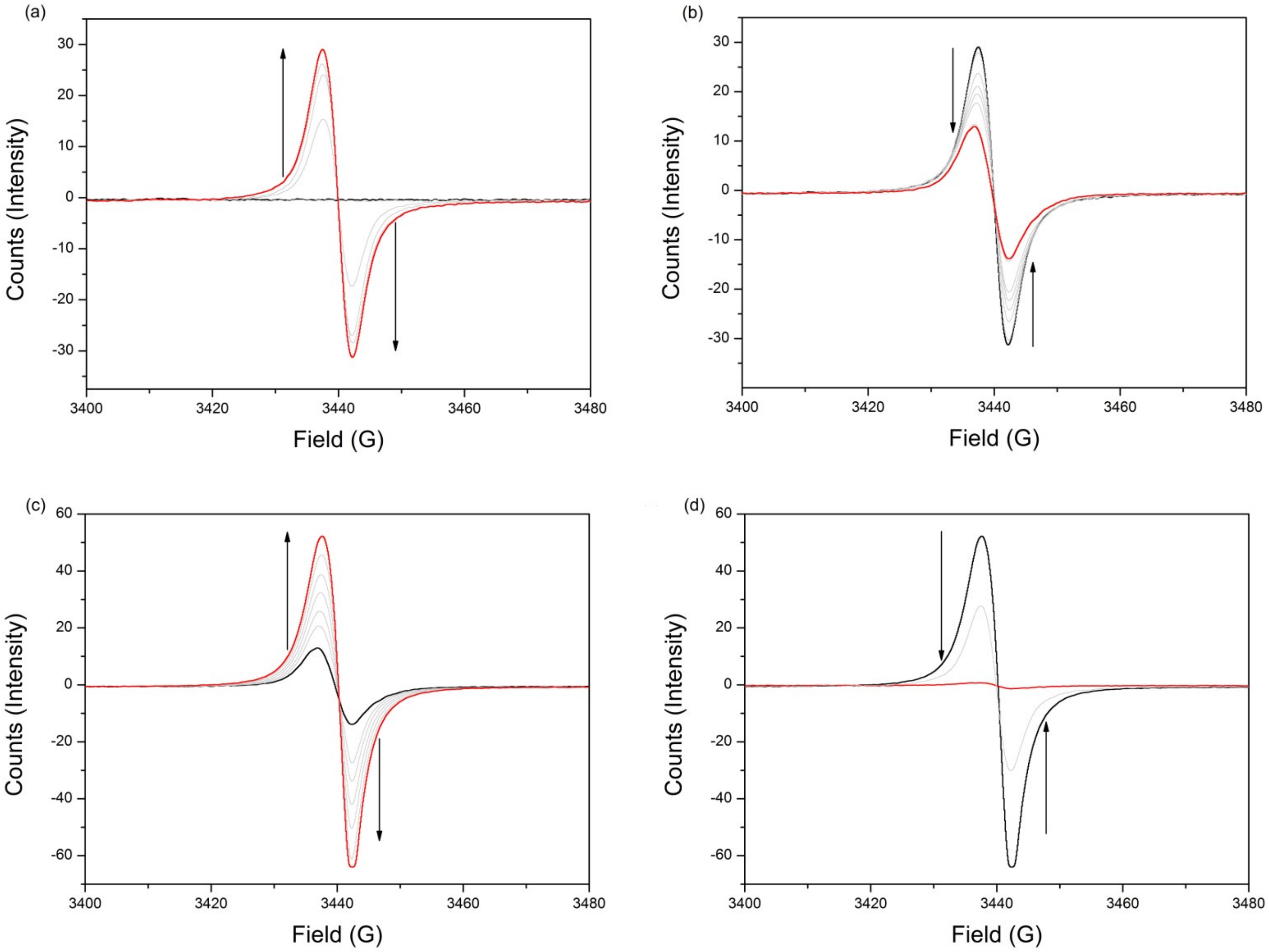

**Figure S6**. Solid state EPR SEC of **DPPTzTz** in 0.1 M [*n*-Bu$_4$N]PF$_6$ / MeCN, showing progression of the TzTz organic radical signal at $g = 2.0051$ at an applied potential of (a) -2.2 V; (b) -2.4 V; and upon returning the applied to (c) -2.0 V; and (d) 0 V, against Ag/Ag$^+$. Arrows represent direction of spectral progression.

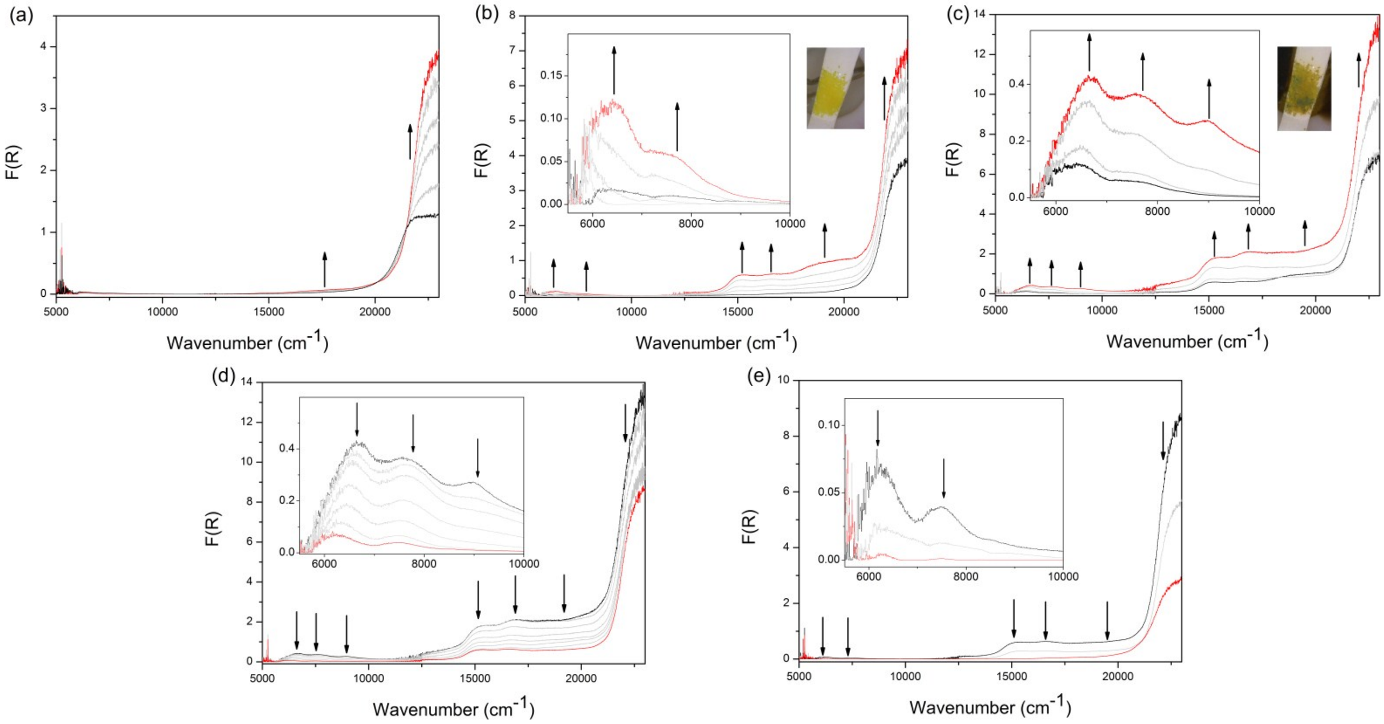

**Figure S7**. Solid state UV-Vis-NIR SEC of **1-Zn** in 0.1 M [$n$-Bu$_4$N]PF$_6$ / MeCN with arrows indicating spectral progression of bands at an applied potential of (a) -1.6 V; (b) -2.1 V; (c) -2.4 V; (d) holding at -2.4 V; and (e) upon returning to 0 V, against Ag/Ag$^+$. Insets show the corresponding NIR region.

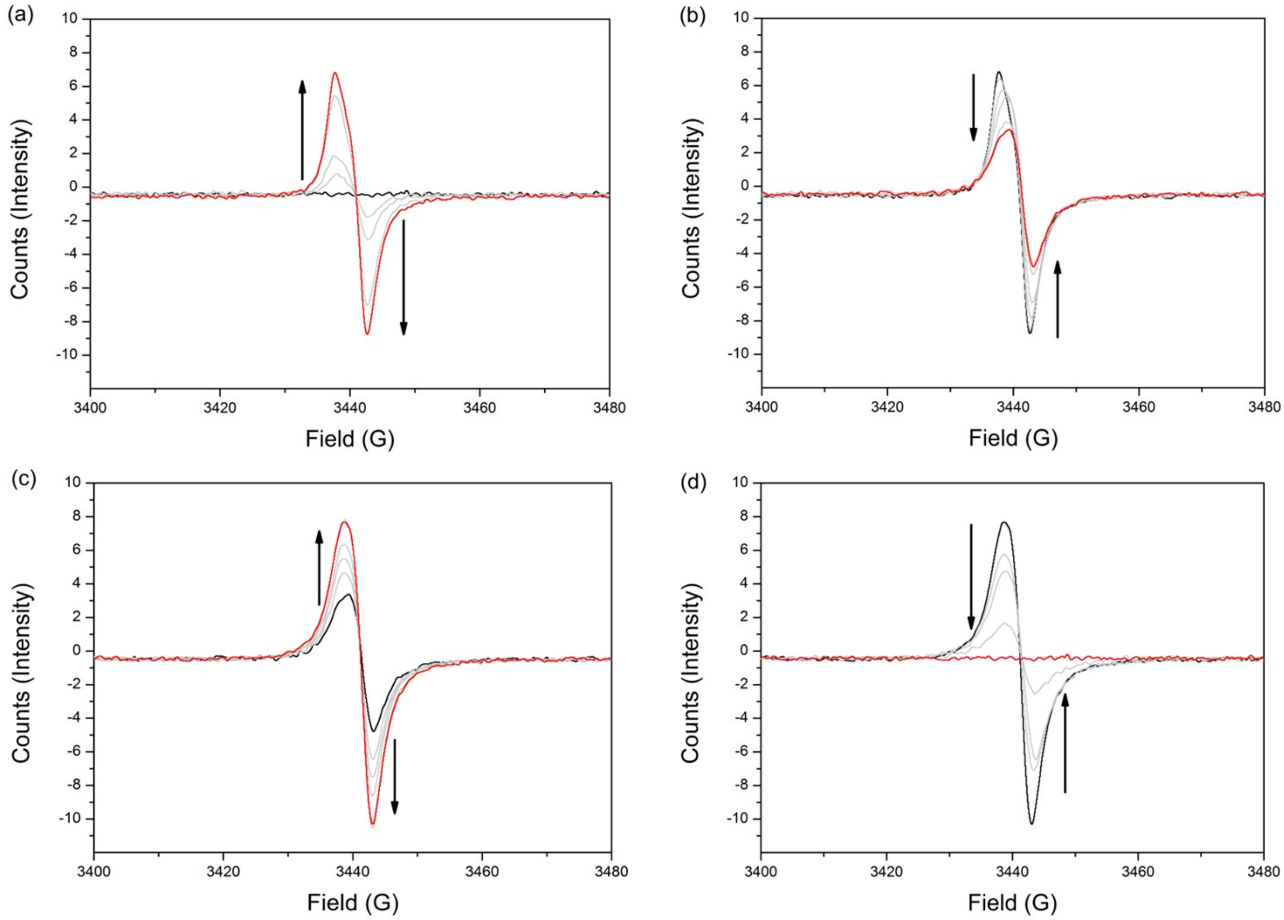

**Figure S8**. Solid state EPR SEC of **1-Zn** in 0.1 M [$n$-Bu$_4$N]PF$_6$ / MeCN, showing progression of the TzTz organic radical signal at $g$ = 2.0043 at an applied potential of (a) -1.8 V; (b) -2.1 V; (c) -2.4 V; and (d) upon returning the applied potential to 0 V, against Ag/Ag$^+$. Arrows represent direction of spectral progression.

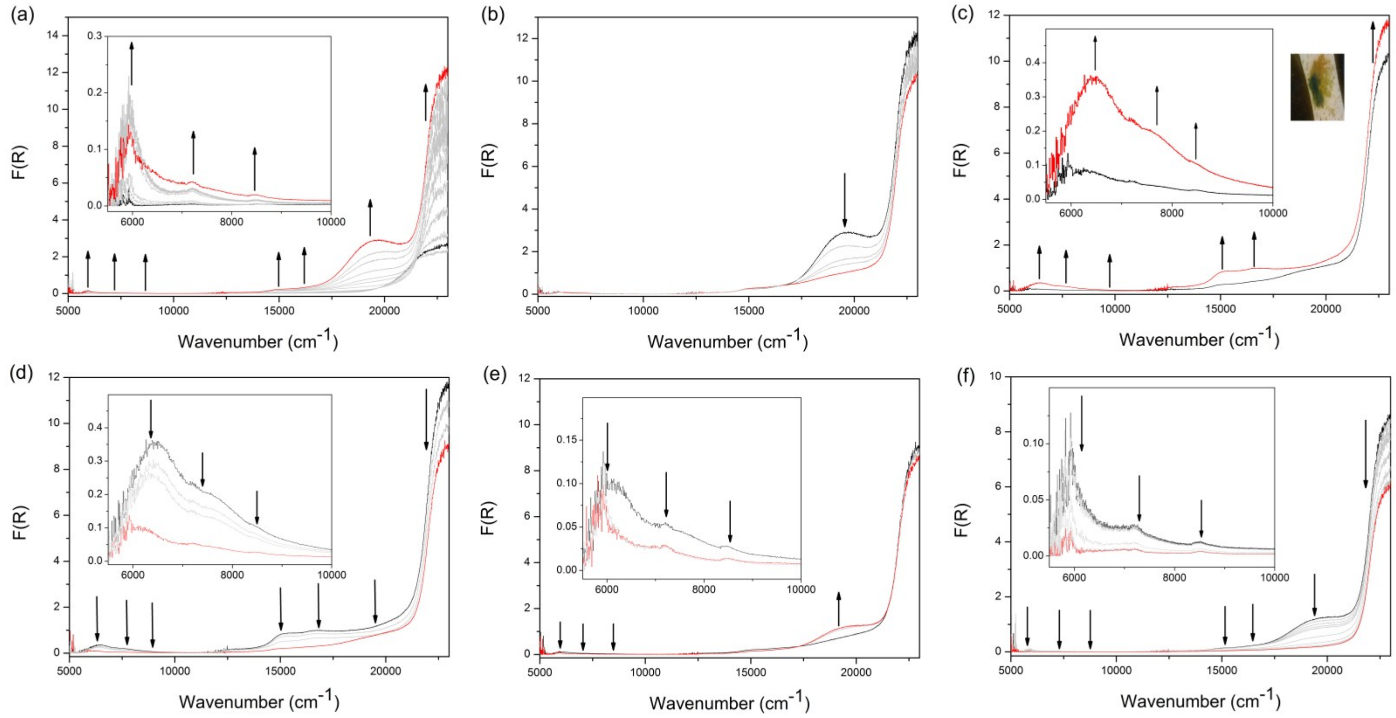

**Figure S9**. Solid state UV-Vis-NIR SEC of **2-Cd** in 0.1 M [$n$-Bu$_4$N]PF$_6$ / MeCN with arrows indicating spectral progression of bands at an applied potential of (a) -2.1 V; (b) -2.3 V; (c) -2.4 V; (d/e/f) holding at -2.4 V, against Ag/Ag$^+$, with spectral progression documented in (d) upon immediate application; (e) between 20 and 40 mins; and (f) after 40 mins. Insets show the corresponding NIR region.

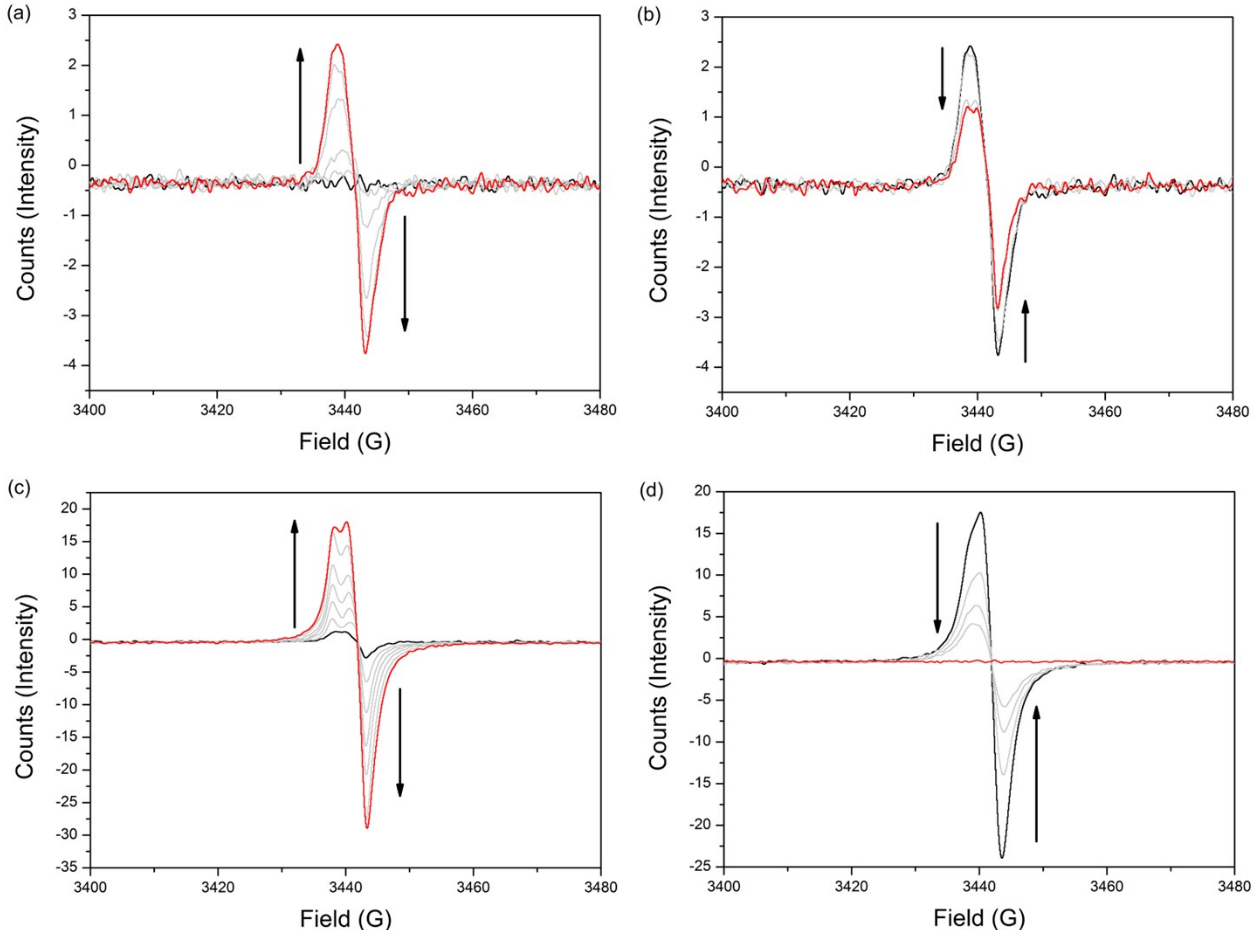

**Figure S10**. Solid State EPR SEC of **2-Cd** in 0.1 M [$n$-Bu$_4$N]PF$_6$ / MeCN, showing progression of the TzTz organic radical signal at $g$ = 2.0037 at an applied potential of (a) -2.0 V; (b) holding at -2.0 V; (c) -2.4 V; and (d) upon returning to 0V, against Ag/Ag$^+$. Arrows represent direction of spectral progression.

**Table S3**. Calculated proportion of Li/Zn and Li/Cd giving the actual state of reduction in **1-Zn** and **2-Cd** reduced samples respectively, calculated from ICP-AES analysis of the wt% of Zn or Cd and Li in each respective sample.

| Sample | Theoretical Li against Zn/Cd ratio | Li against Zn/Cd ratio | Molecular formula |
|---|---|---|---|
| **1-Zn-Red1** | 0.50 | 0.431 | $[Zn_2Li_{0.86}(DPPTzTz)_2(SDC)_2]_n$ |
| **1-Zn-Red2** | 1.0 | 0.706 | $[Zn_2Li_{1.4}(DPPTzTz)_2(SDC)_2]_n$ |
| **1-Zn-Red3** | 2.0 | 0.973 | $[Zn_2Li_{1.9}(DPPTzTz)_2(SDC)_2]_n$ |
| **1-Zn-Red4** | 3.0 | 1.96 | $[Zn_2Li_{3.9}(DPPTzTz)_2(SDC)_2]_n$ |
| **2-Cd-Red1** | 0.50 | 0.342 | $[Cd_2Li_{0.68}(DPPTzTz)_2(SDC)_2]_n$ |
| **2-Cd-Red2** | 1.0 | 0.568 | $[Cd_2Li_{1.1}(DPPTzTz)_2(SDC)_2]_n$ |
| **2-Cd-Red3** | 2.0 | 0.798 | $[Cd_2Li_{1.6}(DPPTzTz)_2(SDC)_2]_n$ |
| **2-Cd-Red4** | 3.0 | 0.832 | $[Cd_2Li_{1.7}(DPPTzTz)_2(SDC)_2]_n$ |

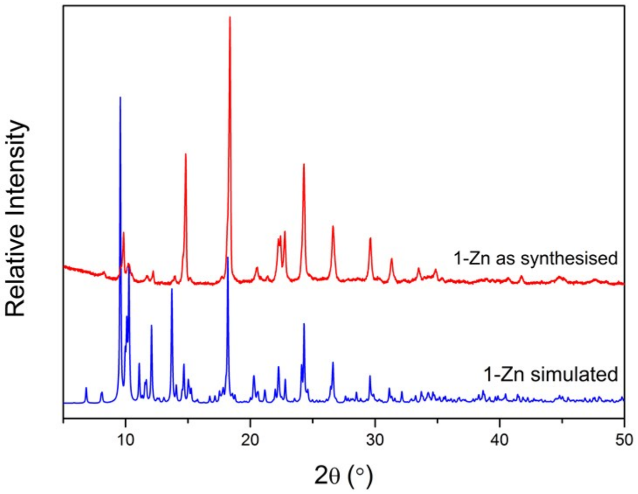

**Figure S11**. PXRD pattern of **1-Zn** as synthesised (red) in comparison with its simulated pattern (blue) calculated from its crystal structure.

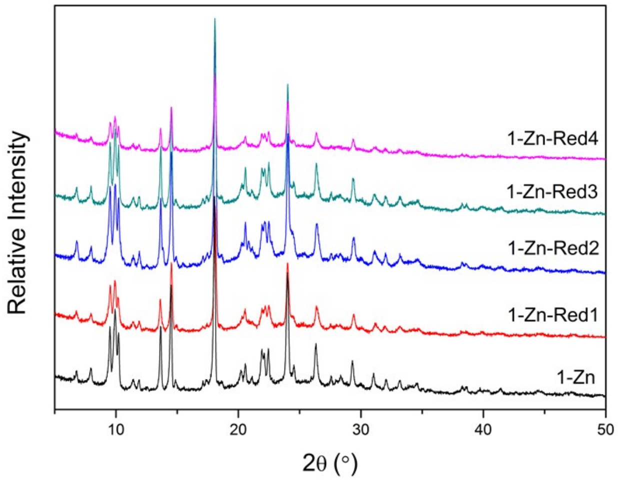

**Figure S12**. PXRD pattern of reduced samples of **1-Zn**, compared to the neutral state as synthesised pattern.

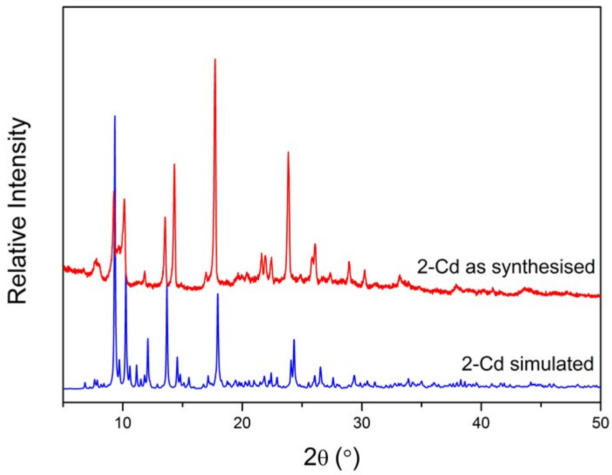

**Figure S13**. PXRD pattern of **2-Cd** as synthesised (red) in comparison with its simulated pattern (blue) calculated from its crystal structure.

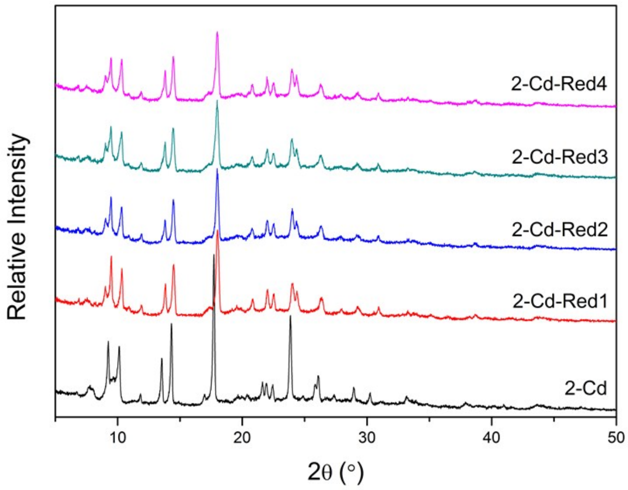

**Figure S14**. PXRD pattern of reduced samples of **2-Cd**, compared to the neutral state as synthesised pattern.

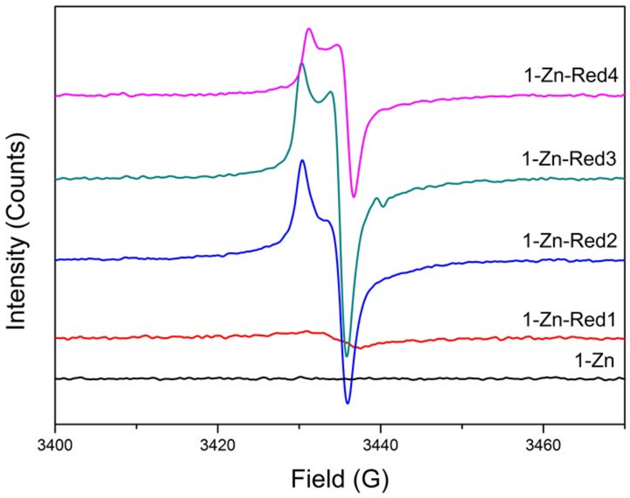

**Figure S15**. Solid state EPR of **1-Zn** neutral and reduced frameworks.

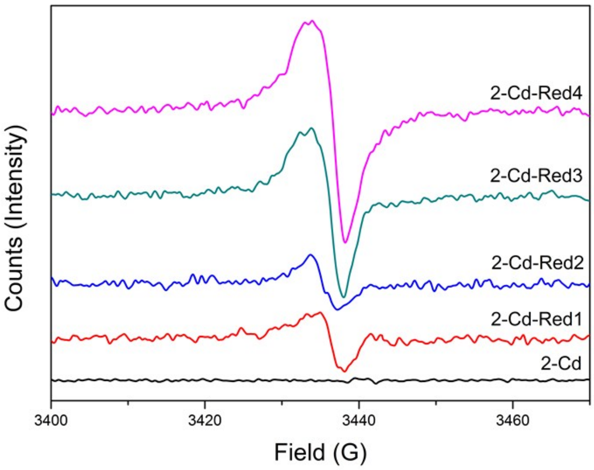

**Figure S16**. Solid state EPR of **2-Cd** neutral and reduced frameworks.

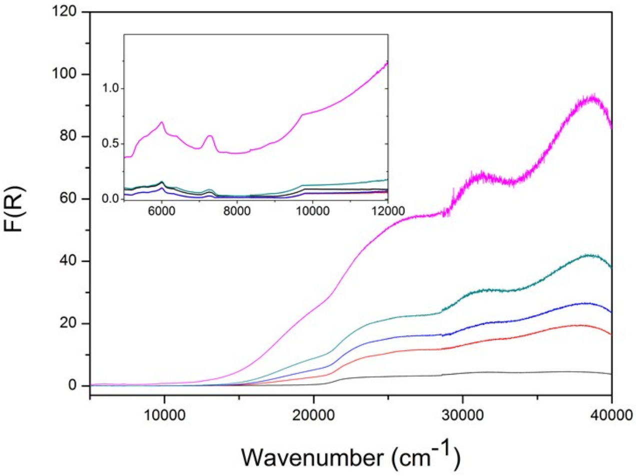

**Figure S17**. Solid state UV-Vis-NIR spectra over the range 5000 to 40000 cm$^{-1}$ of **1-Zn** (black), **1-Zn-Red1** (red), **1-Zn-Red2** (blue), **1-Zn-Red3** (cyan) and **1-Zn-Red4** (magenta), with inset showing the NIR region.

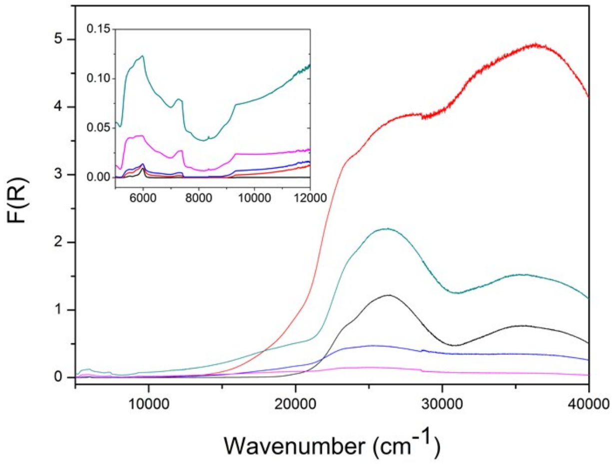

**Figure S18**. Solid state UV-Vis-NIR spectra over the range 5000 to 40000 cm$^{-1}$ of **1-Cd** (black), **1-Cd-Red1** (red), **1-Cd-Red2** (blue), **1-Cd-Red3** (cyan) and **1-Cd-Red4** (magenta), with inset showing the NIR region.

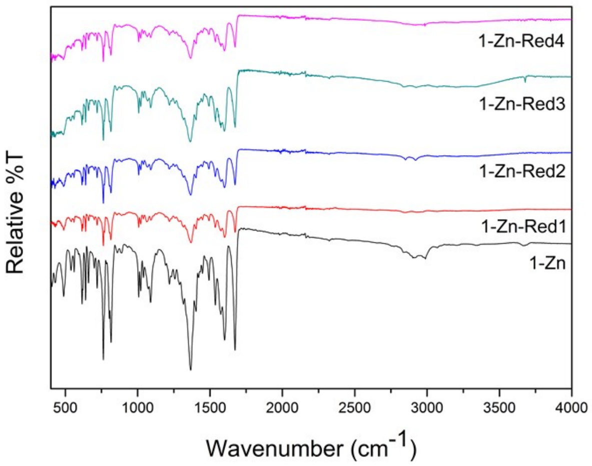

**Figure S19**. FT-IR of **1-Zn** neutral and reduced frameworks.

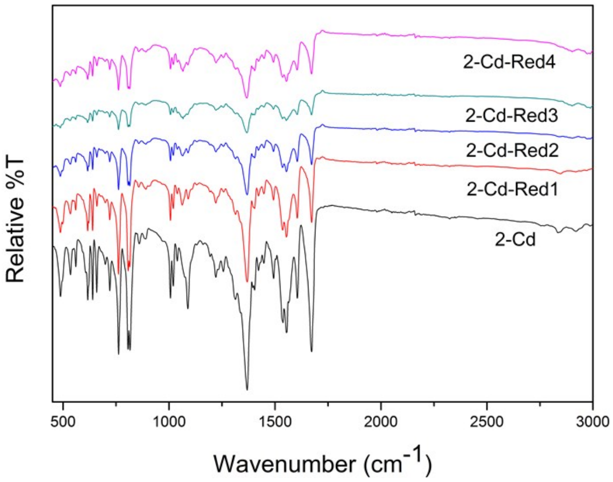

**Figure S20**. FT-IR of **2-Cd** neutral and reduced frameworks.

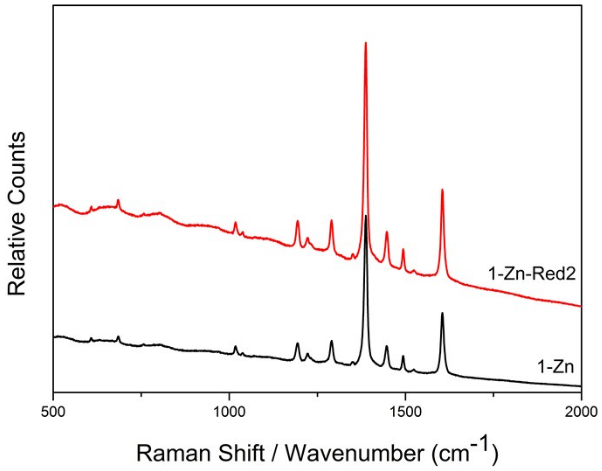

**Figure S21**. Raman spectra of **1-Zn** compared with that of **1-Zn-Red2**, obtained by illuminating with an 833 nm laser.

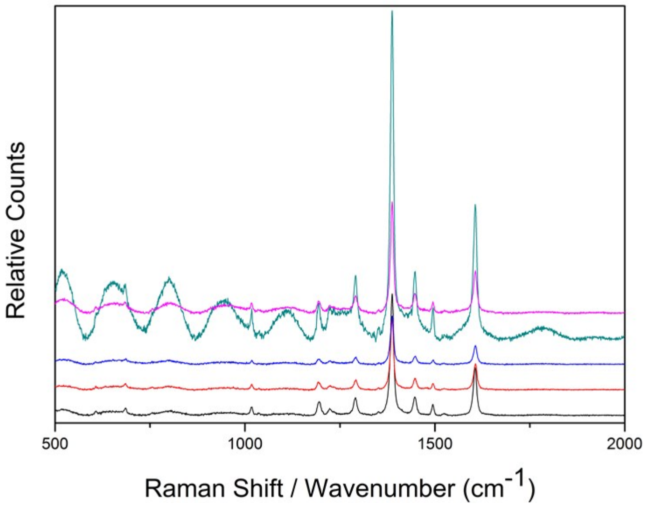

**Figure S22**. Raman spectra of **2-Cd** (black) compared with that of reduced samples **2-Cd-Red1** (red), **2-Cd-Red2** (blue), **2-Cd-Red3** (cyan) and **2-Cd-Red4** (magenta), obtained using an 833 nm excitation wavelength.

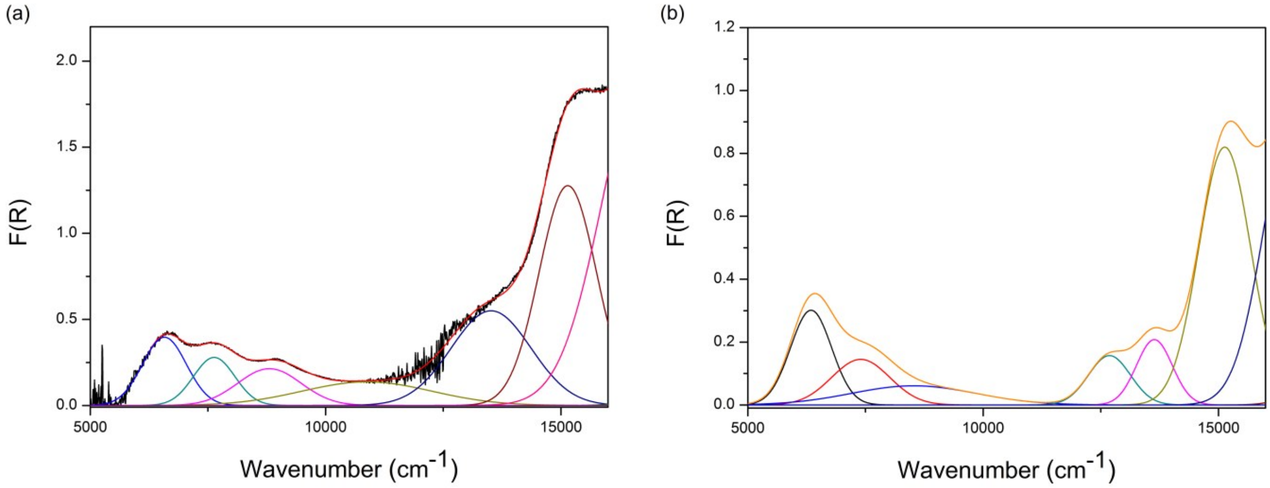

**Figure S23**. Deconvoluted spectrum from 5000 cm$^{-1}$ to 16000 cm$^{-1}$ from the UV-Vis-NIR SEC of (a) **1-Zn** and (b) **2-Cd**, at an applied potential of -2.4 V (with IVCT bands at their maximum values).

## EQUATIONS USED FOR CALCULATIONS

**Eqn 1:** $\Delta v_{\frac{1}{2}} = [16RTln2(v_{max})]^{\frac{1}{2}}$, where the value of $16RTln2$ is 2310 $cm^{-1}$ at 300 K, and $v_{max}$ is the position of the relevant NIR IVCT band.

**Eqn 2:** $H_{ab} = \frac{0.0205 \times \sqrt{v_{max}\varepsilon_{max}\Delta v_{\frac{1}{2}}}}{r}$, where $\varepsilon_{max}$ is the molar extinction coefficient of the relevant IVCT band and $r$ is the distance in Ångstrom between the cofacial dimer pairs.

**Eqn 3:** $T_{da} = \frac{\sqrt{4.2 \times 10^{-4} \times \varepsilon_{max}\Delta v_{\frac{1}{2}}E_{op}}}{d}$, where $E_{op}$ is the optical energy associated with IVCT, which in this instance is given by the energy of the NIR IVCT band. This relationship was developed from classical theory by Hush, and for all applicable values (including in equations 5 and 6), units of $10^3$ $cm^{-1}$ in place of $cm^{-1}$ have been used.

**Eqn 4:** $v_{et} = \frac{4\pi^2 {T_{da}}^2}{h}\sqrt{\frac{\pi}{k_B T\lambda}}$, where $h = 4.136 \times 10^{-15}\ eV.s$ is Planck's constant, $k_B = 8.617 \times 10^{-5}\ eV.K^{-1}$ is the Boltzmann constant, temperature $T = 300$ K and $\lambda$ is the energy of electron transfer (given by the position of the NIR IVCT band) in $eV$.

**Eqn 5:** $k = v_{et}\, e^{\frac{-\chi}{4RT}}$, where $R = 8.314\ \times 6.242 \times 10^{18}\ eV.K^{-1}.mol^{-1}$ is the ideal gas constant and $\chi$ is the molar energy of electron transfer given by multiplying $\lambda$ with Avogadro's constant.

## KUBELKA-MUNK THEORY AND QUANTIFICATION OF THE NEAR-INFRARED (NIR) IVCT BAND

One of the major obstacles to quantifying spectroscopic data for MOFs and ultimately applying Marcus-Hush theory to for electron transfer lies in their insolubility. Solution state spectroscopy allows the straightforward collection of transmission and absorbance data, from which the molar extinction coefficient of various bands can be calculated using the Beer-Lambert law. Solid state samples on the other hand, have far greater scattering coefficients, which not only hinders the accuracy of spectroscopic acquisitions and subsequent application of the Beer-Lambert law, but also introduces another degree of difficulty in consistent sample preparation since particle size effects are important.

The development of Kubelka-Munk (K-M) theory can be considered one of the first steps towards quantifying solid state data.[3] The K-M equation is given as:

$$F(R) = \frac{(1 - R)^2}{2R}$$

where R is the reflectance and F(R) is the transformed units of Kubelka-Munk. This allows the conversion of solid state diffuse reflectance data to an absorbance type plot and allows comparisons to be drawn easily, however, any comparisons made with data transformed with this equation remain semi-qualitative. The K-M equation was derived by treating radiation passing through a sample as consisting of an incident beam, and a reflected beam in the opposite direction, taking into consideration scattering and absorption. From this model, a differential equation was derived which was subsequently integrated to obtain the K-M equation, with the assumption that the sample is infinitely thick, impeding the transmission of light. While this is far from the case in reality, there are a small number of examples where this equation has been used to quantify solid state reflectance data.[4] These examples required the application of specialised equipment involving a full integrating sphere, where reflectance in all directions is accounted for.

Modifications to the popular K-M equation exist, and these have already been applied in the field of paints, primarily to measure the thickness of samples. The most noteworthy example is from a publication by Kubelka,[5] where the same differential equation as used to derive the K-M equation was applied, however by integrating this over a finite domain, a series of relationships between transmittance, reflectance and absorbance of a solid state sample were obtained. Of these, the most important relationships for quantifying solid state reflectance data are:

$$R = \frac{\sinh(bSX)}{a\sinh(bSX) + b\cosh(bSX)}$$

$$SX = \frac{\operatorname{arcsinh}\left(\frac{b}{T}\right) - \operatorname{arcsinh}(b)}{b}$$

$$T^2 + b^2 = (a - R)^2$$

$$a = \frac{S+K}{S}, \quad b = \sqrt{a^2 - 1}$$

where $R = \frac{\%R}{100}$, $T = \frac{\%T}{100}$, S is the scattering coefficient, X is the sample thickness and K is the absorption coefficient. In the first relationship, reflectivity is linked to scattering and absorption coefficients as well as to the sample thickness or pathlength. Next the scattering coefficient of a sample and the pathlength, multiplied together to form a "scattering power SX", is related to its absorption coefficient and transmission. Transmission and reflectance are then both linked to scattering and absorption coefficients, with the representation of scattering and absorption coefficients in a combined "a" and "b" form given in the final line. The only assumption made during the derivation of these relationships was that the sample displayed homogeneous and spectrally non-selective scattering properties. By applying these relationships, in conjunction with computational calculation software such as Wolfram Mathematica, solid state reflectance data can be converted to transmission data, allowing the molar extinction coefficient of various bands to be determined comparatively against a suitable standard.

In the present exercise, quantification of the NIR bands was achieved via a comparison with the molar extinction constant of the UV-Vis π to π* band at 22680 $cm^{-1}$ of the neutral frameworks, using the *in situ* SEC data. First, quantification of the UV-Vis π to π* band at 22680 $cm^{-1}$ was achieved using transmission measurements on KBr pellets containing the frameworks at various concentrations. The percent transmission (%T) values for each pellet were then transformed to an absorbance value (A) using $A = 2 - \log(\%T)$. Although this does not account for scattering, the application of this equation resulted in data sufficient for Marcus-Hush analysis as detailed in the subsequent section. In order to prevent excessive overestimation caused by scattering, pellets containing lower concentrations of the framework were used to measure the molar extinction coefficient. The converted absorbance values for each pellet at 22680 $cm^{-1}$ were then divided by the pellet thickness (cm) and plotted against pellet concentration (calculated in molarity (M) by converting mass to volume by applying the density of KBr) to obtain the molar extinction coefficient of the UV-Vis π to π* bands as the gradient of the line of best fit of the resulting plot, applying the Beer-Lambert law (Figure S21).

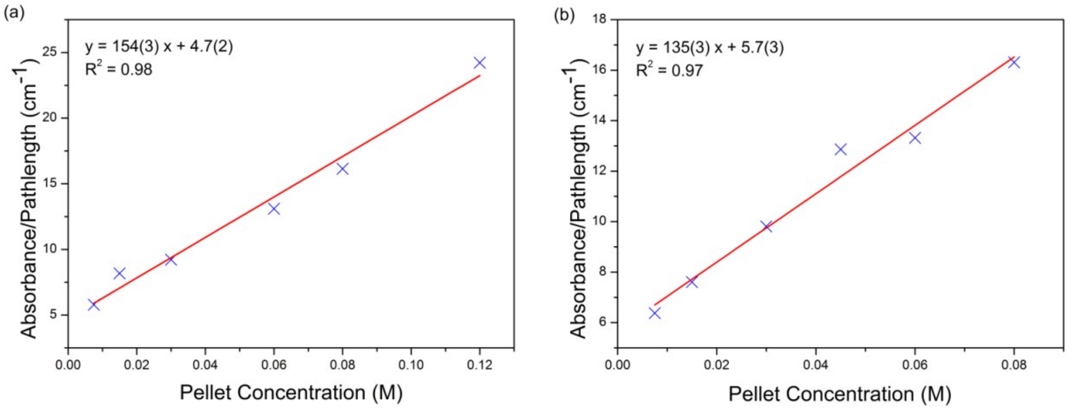

**Figure S24**. Plot of pellet concentration against absorbance divided by pathlength (pellet thickness) for different KBr pellets of the (a) **1-Zn**; and (b) **2-Cd** frameworks.

**Table S4**. Summary of values obtained from calculations obtaining the molar extinction coefficient of the NIR IVCT band from that of the $\pi \rightarrow \pi^*$ band form both **1-Zn** and **2-Cd**.

| **Units** | **1-Zn** | | **2-Cd** | |
|---|---|---|---|---|
| | Neutral State 22680 $cm^{-1}$ band | Deconvoluted NIR IVCT band 6580 $cm^{-1}$ | Neutral State 22680 $cm^{-1}$ band | Deconvoluted NIR IVCT band 6340 $cm^{-1}$ |
| **Kubelka-Munk (F(R))** | 1.277 | 0.3965 | 2.268 | 0.3014 |
| **%Reflectance** | 23.13 | 42.17 | 15.60 | 46.85 |
| **%Transmission** | 17.97 | 48.59 | 13.23 | 74.56 |
| **Absorbance** | 0.7454 | 0.3135 | 0.8784 | 0.1275 |

The molar extinction coefficients of the NIR IVCT bands were then determined by correlating the converted absorbance value to that of the UV-Vis $\pi$ to $\pi^*$ bands at 22680 $cm^{-1}$ from SEC data, with known extinction coefficients. For solid state SEC data, in order to derive the %T value of a sample from its %R value, the scattering power '*Sx*' of a sample was first calculated. As defined above, this is assumed to remain constant for all wavenumbers and reductive states of the framework, thus it was calculated from the neutral state %T (data collected separately from the SEC experiment) and %R data for the $\pi$ to $\pi^*$ band of both frameworks at 22680 $cm^{-1}$, by applying: $T^2 + b^2 = (a - R)^2$ and $SX = \frac{\operatorname{arcsinh}\left(\frac{b}{T}\right) - \operatorname{arcsinh}(b)}{b}$ where $b = \sqrt{a^2 - 1}$. The scattering power of the sample was calculated using Mathematica to be $SX = 0.843$ for **1-Zn** and $SX = 0.651$ for **2-Cd**. This was then applied into the relationship $R = \frac{\sinh(bSX)}{a\sinh(bSX) + b\cosh(bSX)}$ which allowed the subsequent calculation of 'a' representing the scattering and absorption coefficients at each wavenumber from %R data for both frameworks. With knowledge of the value of 'a' at different wavenumbers, this was applied to the $T^2 + b^2 = (a - R)^2$ relationship along with the known %R at each wavenumber to obtain the %T value at any wavenumber from SEC data of both **1-Zn** and **2-Cd**. To ensure that the transformation functions were smooth and well-behaved in the relevant domains, a transformation of neutral state %R to %T of data points on the UV-Vis $\pi$ to $\pi^*$ bands of both frameworks were first performed, and compared to that of the experimentally obtained %T values. These were shown to be within good agreement.

Then, the corresponding %T value for the reduced state IVCT bands were calculated from the electrochemically reduced SEC data, using the same scattering power constants for both **1-Zn** and **2-Cd** as calculated above, and then applying the exact same set of relationships outlined. These values were subsequently converted to an absorbance along with the %T values of the 22680 $cm^{-1}$ bands using $A = 2 - log(\%T)$ to obtain absorbance values for both **1-Zn** and **2-Cd** NIR IVCT bands as well as the respective 22680 $cm^{-1}$ bands for both frameworks. Multiplication of the respective molar extinction coefficient of the 22680 $cm^{-1}$ band for either framework with the ratio of the absorbance of the NIR IVCT band and corresponding absorbance of the 22680 $cm^{-1}$ band yielded the molar extinction coefficient of the NIR IVCT bands as 64.8 $cm^{-1}$ $M^{-1}$ for **1-Zn** and 19.6 $cm^{-1}$ $M^{-1}$ for **2-Cd**. These were then applied into the charge transfer theory equations as outlined in the main body without any further manipulation.

## PXRD REFINEMENTS

**Table S5**. Simulated Pawley cell parameters for **1-Zn**.

| Sample | Space Group | a (Å) | b (Å) | c (Å) | *β* (°) | V (Å$^3$) | R$_{wp}$ (%) |
|---|---|---|---|---|---|---|---|
| **1-Zn** | $P2_1/c$ | 25.84(1) | 18.50(1) | 15.93(1) | 91.24(1) | 7615.0(15) | 13.60 |
| **1-Zn-Red1** | $P2_1/c$ | 25.86(1) | 18.51(1) | 15.98(1) | 91.46(1) | 7646.7(11) | 8.29 |
| **1-Zn-Red2** | $P2_1/c$ | 25.84(1) | 18.52(1) | 15.93(1) | 91.32(1) | 7624.7(13) | 11.84 |
| **1-Zn-Red3** | $P2_1/c$ | 25.86(1) | 18.51(1) | 15.94(1) | 91.38(1) | 7626.0(22) | 10.21 |
| **1-Zn-Red4** | $P2_1/c$ | 25.84(1) | 18.49(1) | 15.93(1) | 91.40(1) | 7610.2(20) | 8.29 |

**Table S6**. Simulated Pawley cell parameters for **2-Cd**.

| Sample | Space Group | a (Å) | b (Å) | c (Å) | *α* (°) | *β* (°) | *γ* (°) | V (Å$^3$) | R$_{wp}$ (%) |
|---|---|---|---|---|---|---|---|---|---|
| **2-Cd** | *P*-1 | 16.19(1) | 19.02(1) | 26.08(1) | 88.46(1) | 87.58(1) | 90.02(1) | 8023.9(12) | 10.77 |
| **2-Cd-Red1** | *P*-1 | 15.86(1) | 19.11(1) | 26.10(1) | 82.10(1) | 87.17(1) | 89.65(1) | 7822.0(16) | 7.87 |
| **2-Cd-Red2** | *P*-1 | 15.87(1) | 19.12(1) | 26.10(1) | 82.13(1) | 87.23(1) | 89.46(1) | 7833.5(15) | 8.66 |
| **2-Cd-Red3** | *P*-1 | 15.85(1) | 19.11(1) | 26.09(1) | 82.18(1) | 87.14(1) | 89.46(1) | 7818.7(15) | 7.08 |
| **2-Cd-Red4** | *P*-1 | 15.85(1) | 19.15(1) | 26.15(1) | 82.10(1) | 87.13(1) | 89.48(1) | 7849.6(13) | 6.62 |

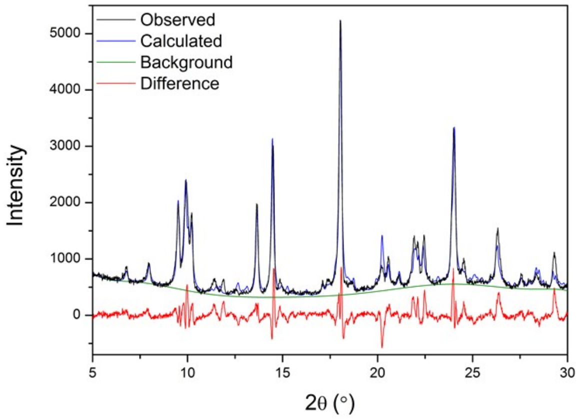

**Figure S25**. Pawley extraction of **1-Zn**.

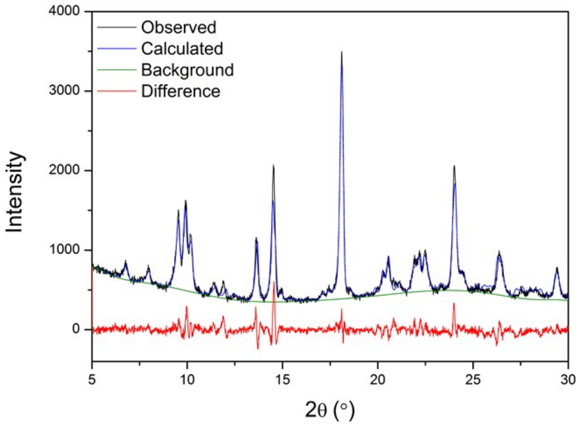

**Figure S26**. Pawley extraction of **1-Zn-Red1**.

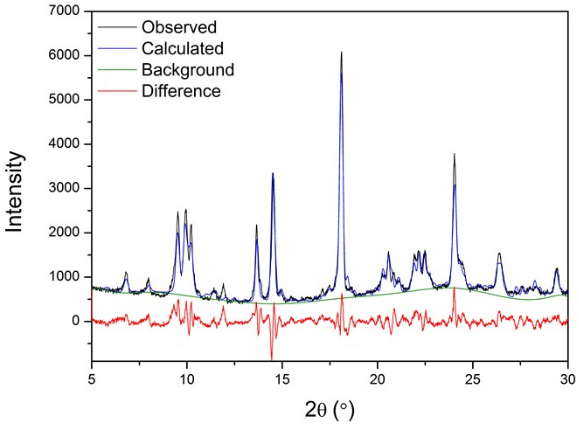

**Figure S27**. Pawley extraction of **1-Zn-Red2**.

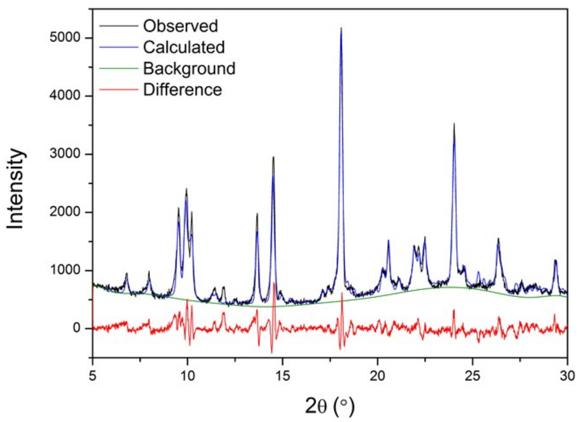

**Figure S28**. Pawley extraction of **1-Zn-Red3**.

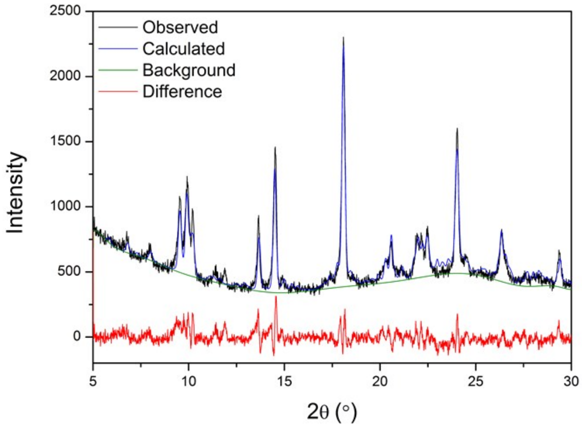

**Figure S29**. Pawley extraction of **1-Zn-Red4**.

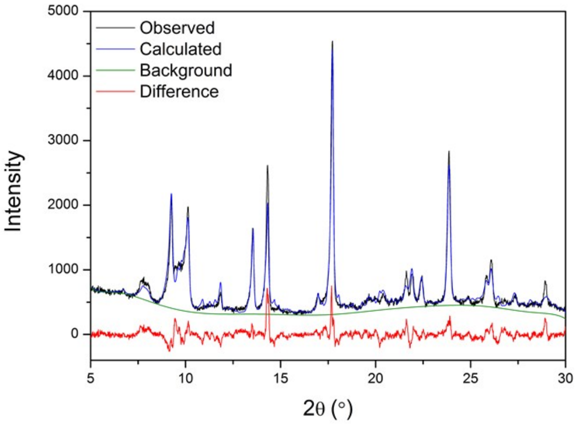

**Figure S30**. Pawley extraction of **2-Cd**.

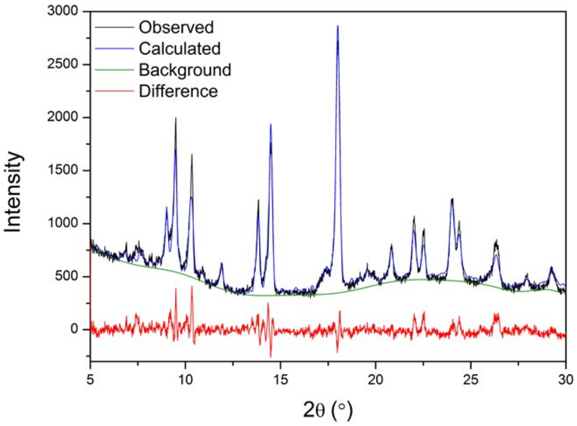

**Figure S31**. Pawley extraction of **2-Cd-Red1**.

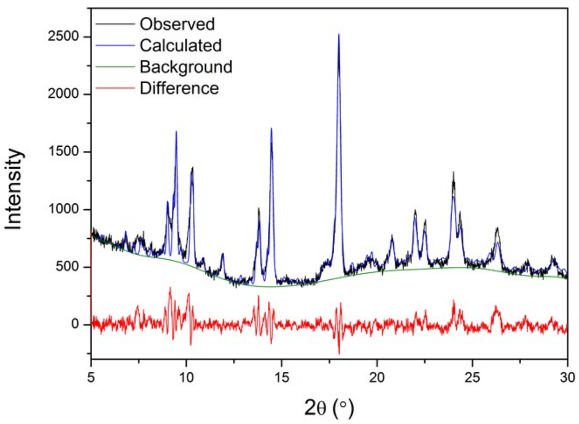

**Figure S32**. Pawley extraction of **2-Cd-Red2**.

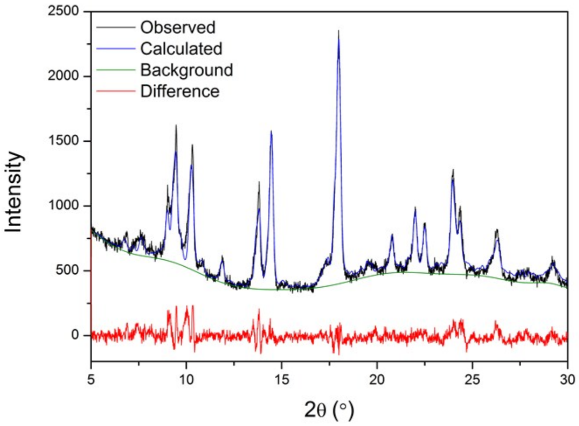

**Figure S33**. Pawley extraction of **2-Cd-Red3**.

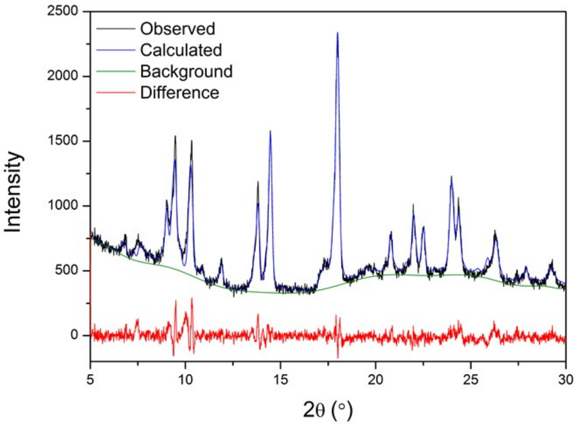

**Figure S34**. Pawley extraction of **2-Cd-Red4**.

## REFERENCES

1. B. Wang, P. Ni, J. Fan, H. Zheng, S. Zhao and Z. Bai, *Chin. J. Org. Chem.*, 2014, **34**, 2471.
2. Y.J. Hwang, T. Earmme, B.A.E. Courtright, F.N. Eberle and S.A. Jenekhe, *J. Am. Chem. Soc.*, 2015, **137**, 4424.
3. P. Kubelka and F. Munk, *Zeitschrift fur Technische Physik* 1931, **12**, 593.
4. U. Schroder and F. Scholz, *J. Solid State Electrochem.* 1997, **1**, 62.
5. P. Kubelka, *J. Opt. Soc. Am.* 1948, **38**, 448.